

YOUNG REMNANTS OF TYPE IA SUPERNOVAE AND THEIR PROGENITORS: A STUDY OF SNR G1.9+0.3

SAYAN CHAKRABORTI¹, FRANCESCA CHILDS², AND ALICIA SODERBERG³

Institute for Theory and Computation, Harvard-Smithsonian Center for Astrophysics, 60 Garden Street, Cambridge, MA 02138, USA

Draft version November 2, 2015

ABSTRACT

Type Ia supernovae, with their remarkably homogeneous light curves and spectra, have been used as standardizable candles to measure the accelerating expansion of the Universe. Yet, their progenitors remain elusive. Common explanations invoke a degenerate star (white dwarf) which explodes upon reaching close to the Chandrasekhar limit, by either steadily accreting mass from a companion star or violently merging with another degenerate star. We show that circumstellar interaction in young Galactic supernova remnants can be used to distinguish between these single and double degenerate progenitor scenarios. Here we propose a new diagnostic, the Surface Brightness Index, which can be computed from theory and compared with Chandra and VLA observations. We use this method to demonstrate that a double degenerate progenitor can explain the decades-long flux rise and size increase of the youngest known Galactic SNR G1.9+0.3. We disfavor a single degenerate scenario. We attribute the observed properties to the interaction between a steep ejecta profile and a constant density environment. We suggest using the upgraded VLA to detect circumstellar interaction in the remnants of historical Type Ia supernovae in the Local Group of galaxies. This may settle the long-standing debate over their progenitors.

Subject headings: ISM: supernova remnants — radio continuum: general — X-rays: general — binaries: general — circumstellar matter — supernovae: general — ISM: individual objects(SNR G1.9+0.3)

1. INTRODUCTION

Type I supernovae were classified by Minkowski (1941) to be a largely homogeneous group characterized by the lack of Hydrogen in their spectra. A major subset called Type Ia, which have early-time spectra with strong Si II (Filippenko 1997), are believed to come from the thermonuclear explosions of degenerate stellar cores (Wheeler & Harkness 1990). Despite their homogeneity, peak absolute magnitudes of Type Ia supernovae are not constant. Phillips (1993) related their peak brightness to the width of their light curve. This allowed Riess et al. (1996) to standardize them as reliable distance indicators. Type Ia supernovae have been used as standard candles, leading to the discovery of the accelerating expansion of the Universe (Riess et al. 1998; Schmidt et al. 1998; Perlmutter et al. 1999). As a consequence of their importance in astronomy and cosmology, Type Ia supernovae are the subject of various theoretical and observational studies. Yet, much remains to be known of the stellar systems that produce these explosions.

It is generally agreed upon (Hillebrandt & Niemeyer 2000) that Type Ia supernovae mark catastrophic explosions of white dwarfs near and or above the Chandrasekhar (1931) limit. Accreted mass, required to destabilize the white dwarf, is transferred from a binary companion whose nature is as yet unknown. The single degenerate (SD) model (Whelan & Iben 1973; Nomoto

1982) uses a progenitor system with a white dwarf and a non-degenerate companion. The companion can be a main-sequence, sub-giant, He star, or red-giant. In contrast, the double degenerate (DD) model (Webbink 1984; Iben & Tutukov 1984) relies on the merging of two white dwarfs.

Red supergiant progenitors of Type IIP supernovae (Smartt et al. 2009) have been identified in pre-explosion images of host galaxies. Chevalier et al. (2006) suggested using the interaction of the supernova ejecta with the circumstellar matter as a probe of mass loss from these red supergiants. Circumstellar interaction is now being used to constrain the nature of Type IIP supernova progenitors (Chakraborti et al. 2012, 2013, 2015).

Unlike the massive stellar progenitors of core collapse supernovae, many of the putative progenitors for Type Ia supernovae are too faint to be detected in external galaxies through direct imaging with the present generation of optical telescopes. As a result circumstellar interaction, or lack thereof, is a promising method for discerning the progenitors of Type Ia supernovae. Properties of supernova remnants may provide a consistency check for the models of Type Ia supernova progenitors (Badenes et al. 2007). Circumstellar interaction in Type I supernovae may produce radio emission (Chevalier 1984). Recently, the lack of such early radio (Chomiuk et al. 2012; Horesh et al. 2012) and X-ray (Margutti et al. 2012) emission, from Type Ia SN 2011fe, has ruled out much parameter space for SD scenarios. We seek to extend the scope of such studies to young supernova remnants.

We predict temporal evolution of size and optically thin radio and X-ray synchrotron emission from a young supernova remnant. Radio and X-ray lightcurve during

schakraborti@fas.harvard.edu

¹ Society of Fellows, Harvard University, Cambridge, MA 02138, USA

² Harvard College, Harvard University, Cambridge, MA 02138

³ Department of Astronomy, Harvard University, Cambridge, MA 02138, USA

this regime shows distinctly different behavior for SD and DD scenarios. We compare these with long term radio and X-ray observations of the youngest known Galactic supernova remnant, SNR G1.9+0.3. We develop a diagnostic, the Surface Brightness Index, to compare the flux and size evolution. We show that observations are inconsistent with a SD scenario and can be explained by a DD scenario. So we favor a scenario in which two degenerate stars collided in a nearly constant density environment to produce the supernova that made SNR G1.9+0.3. We suggest that the way to discern the progenitor systems of Type Ia supernova remnants is to measure the change in radius and flux over time and then compare them with our models to check which one is favored. We also show that two separate spectral indices should be expected for the X-ray and Radio emission, when considering electron cooling due to synchrotron losses. We find that this effect is also observed in SNR G1.9+0.3.

2. SNR G1.9+0.3

Radio surveys, using the Very Large Array (VLA), identified SNR G1.9+0.3 as the smallest ($R \sim 2$ pc), and therefore possibly the youngest Galactic supernova remnant (Green & Gull 1984). Chandra X-ray Observatory data confirmed that this young remnant is in the freely expanding phase as a X-ray-synchrotron-dominated shell supernova remnant (Reynolds et al. 2008). Subsequent radio and X-ray observations confirmed its expansion and brightening (Green et al. 2008; Borkowski et al. 2014). Spectral variations in X-rays, interpreted in terms of magnetic field obliquity dependence of cosmic ray acceleration, have been used to argue for a Type Ia event (Reynolds et al. 2009). Ejecta distribution asymmetry and inhomogeneous abundances have also been interpreted in context of Type Ia models (Borkowski et al. 2013). Furthermore, the remnant is not associated with any known star-forming region. All these point towards SNR G1.9+0.3 being a young remnant of a thermonuclear supernova; a Galactic Type Ia supernova in the 19th century, unobserved due to the large extinction along the Galactic plane. In this paper we develop a method to discern the progenitor systems of Type Ia remnants and demonstrate it using SNR G1.9+0.3.

3. CIRCUMSTELLAR INTERACTION

Most early emission from supernovae is powered by heating due to radioactive decay. Whereas, most emission from old supernova remnants is powered by cooling of shock heated ejecta and circumstellar matter. Less attention is given to late emission from supernovae and young remnants where radioactive heating becomes less important and is gradually overtaken by circumstellar interaction. SNR G1.9+0.3 provides a unique window into this young remnant stage, where circumstellar interaction is the major source of heating, yet the swept up mass is low enough that the remnant is in nearly free expansion. This allows us to build a simple model for radio synchrotron emission from a young supernova remnant.

3.1. Initial Conditions

We consider a scenario (see Figure 1) where the ejected mass interacts with circumstellar matter at a radius $R(t)$ (Chakraborti & Ray 2011). Following Chevalier (1982b), we label the mass of the shocked circumstellar matter as

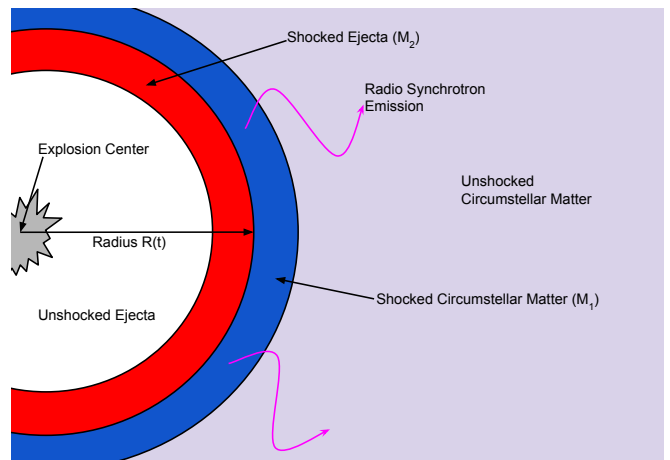


FIG. 1.— Schematic representation of the model used to predict the size and flux density evolution of young supernova remnants. The ejecta and circumstellar matter are heated by shocks at the interaction. A fraction of the thermal energy goes to magnetic fields and accelerated electrons. The synchrotron emission from these electrons drive the flux density evolution.

M_1 , and the shocked ejected mass as M_2 . The density inside the contact discontinuity is ρ_{sn} and the density outside is ρ_{cs} . The circumstellar density profile is different in the SD and DD cases. In the SD case, the density is shaped by the mass loss (\dot{M}) from the wind (with velocity v_w). This can happen in a various ways, such as loss from the outer Lagrange point or the winds driven by accretion on to the degenerate companion. In the DD case, where neither star has appreciable winds, the circumstellar environment is essentially provided by the local density that remains mostly unaltered by the binary and is assumed constant for this simple model.

We express the pre-explosion circumstellar density (ρ_{cs}) at a distance r as,

$$\rho_{cs} \propto r^{-s}. \quad (1)$$

In the above equation, the power law index s is 2 for the SD case and 0 for the DD case. The presence of nova shells do not alter the situation. The age of the remnant under consideration is approximately 150 years (Green et al. 2008) and this is much larger than the time it would take to sweep up the distance between individual shells, which is between 1 and 10 years. Thus, the granularity presented by the shells does not matter in the long term evolution of the size and flux.

We assume that the fastest moving ejecta has a power law density profile,

$$\rho_{sn} \propto v^{-n} t^{-3} \propto r^{-n} t^{n-3}. \quad (2)$$

This substitution is allowed for the ejecta in homologous expansion which has not yet interacted with anything. This allows us to use $v \equiv \frac{r}{t}$. Note that only a small fraction of the matter ejected by the supernova is at the very high velocities. The steepness of this profile is controlled by the power law index n , which must be greater than 5 for the total energy in the ejecta to be finite. Colgate & McKee (1969) suggested profiles with $n = 7$ for an explosion of a high mass white dwarf. Nomoto et al. (1984) used their W7 model to explain the early spectral evolution of Type Ia supernovae. Models like these often had steep ejecta profiles, prompting some authors

to consider exponential profiles (Dwarkadas & Chevalier 1998).

3.2. Blastwave Dynamics

Here we consider the scaling relations of different parameters depending on the circumstellar density profile and the explosion profile. We begin by finding the mass of the shocked circumstellar matter, M_1 as

$$M_1 \propto \int_0^R \rho_{cs} r^2 dr \propto R^{3-s}. \quad (3)$$

This is simply the mass enclosed in the spherical region that has been hollowed out by the explosion. By evaluating the integral we find M_1 's dependence on radius. Next we find the amount of shocked ejected mass M_2 as

$$M_2 \propto \int_R^\infty \rho_{sn} r^2 dr \propto t^{n-3} R^{3-n}. \quad (4)$$

This is the mass that has already interacted with the circumstellar medium and has been slowed down. In the same fashion as before we evaluate the integral to find how M_2 depends on radius.

The next useful quantity to evaluate is the pressure. The pressure that the shocked circumstellar mater exerts P_1 , and the pressure of the ejected mass P_2 , compete to decelerate or accelerate the expansion of the remnant. The pressure provided by the flux of momentum brought in by the matter reaching the contact discontinuity is proportional to the density times the square of the velocity.

$$P_1 \propto \rho_{cs}(R')^2 \propto t^{-2} R^{2-s} \quad (5)$$

$$P_2 \propto \rho_{sn}(R')^2 \propto t^{n-5} R^{2-n} \quad (6)$$

These two equations are simplified by substituting our expressions for the different densities. We also know the shell is decelerating as it interacts with the circumstellar material (Chevalier 1982c). This deceleration is proportional to the difference in pressure times the area of the shell, so

$$(M_1 + M_2)R''(t) \propto R^2(P_2 - P_1). \quad (7)$$

We use this to see how radius scales with time.

$$(M_1 + M_2) \frac{R}{t^2} \propto R^2(P_2 - P_1) \quad (8)$$

Therefore, after plugging in our previous scaling relationships for M_1 , M_2 , P_1 , and P_2 we see that,

$$R \propto t^{\frac{n-3}{n-s}}. \quad (9)$$

We call the power index of this equation m from now on. So,

$$R \propto t^m, \quad (10)$$

where

$$m \equiv \frac{n-3}{n-s}. \quad (11)$$

3.3. Magnetic Fields and Particle Acceleration

Now we use these scaling relations to figure out how the thermal energy, magnetic field, number of accelerated electrons, and finally the flux scale with time. We find the thermal energy by evaluating the kinetic energy lost during the decelerated expansion.

$$E_{th} \propto M_1(R')^2 \propto t^{\frac{(n-5)(3-s)}{n-s}} \quad (12)$$

Note, that in both the SD and DD cases, as long as t is less than the Sedov time, bulk of the energy remains locked up in the kinetic energy of the ejecta. The thermal energy E is lesser than E_0 and steadily increasing during this phase. As more and more gas is shock heated by the circumstellar interaction, a fraction of this energy is made available for magnetic field amplification and cosmic ray acceleration. This is what drives the radio lightcurves of late time supernovae (Chevalier 1982b) and young remnants (Cowsik & Sarkar 1984).

Considering magnetic fields of average strength B , produced by turbulent amplification at shocks, total magnetic energy scales as,

$$E_B \propto B^2 R^3. \quad (13)$$

Following Chevalier (1982b) we consider, that a fraction of the thermal energy goes into producing magnetic fields. Therefore, the magnetic field scales as,

$$B \propto (E_{th} R^{-3})^{1/2} \propto t^{\frac{s(5-n)-6}{2(n-s)}}. \quad (14)$$

We consider a shock accelerated electron distribution where the number density of energetic electrons is given by $N_0 E^{-p} dE dV$. Here N_0 is the normalization of the spectrum of accelerated electron and p is the power law index of the same spectrum. We assume that this distribution extends from $\gamma_m m_e c^2$ to infinity, filling a fraction of the spherical volume of radius R . Therefore the total energy in accelerated electrons scales like,

$$E_e \propto N_0 R^3. \quad (15)$$

Assuming that this represents a fraction of the total thermal energy, we have,

$$N_0 \propto E_{th} R^{-3} \propto t^{\frac{s(5-n)-6}{(n-s)}}. \quad (16)$$

3.4. Synchrotron Emission

Early non-thermal emission from a supernova is often optically thick even at radio radio frequencies, due to free-free or synchrotron self absorption. As the optical thickness reduces with time, the flux density often rises. The peaking of the radio light curve can take days to months depending upon the circumstellar density and expansion velocity. However, late time radio supernovae display optically thin spectra (Chevalier 1982b). Given that the young remnant phase follows after the late supernova phase, we can safely assume that the radio emission (F_ν) at a frequency $\nu \sim 1$ GHz is reasonably approximated by an optically thin spectra.

Following Rybicki & Lightman (1979) and (Chevalier 1982b)

$$F_\nu = \frac{4\pi f R^3}{3D^2} c_5 N_0 B^{(p+1)/2} \left(\frac{\nu}{2c_1} \right)^{-(p-1)/2}, \quad (17)$$

where c_1 and c_5 are constants (Pacholczyk 1970) and D is distance to source. Since we know R , N_0 and B as functions of time, we can calculate how radio flux density scales with time,

$$F_\nu \propto R^3 N_0 B^{7/4} \propto t^{\frac{3(-54+n(8-5s)+25s)}{8(n-s)}}. \quad (18)$$

We will call the power index of time in the above equation β . So,

$$F_\nu \propto t^\beta, \quad (19)$$

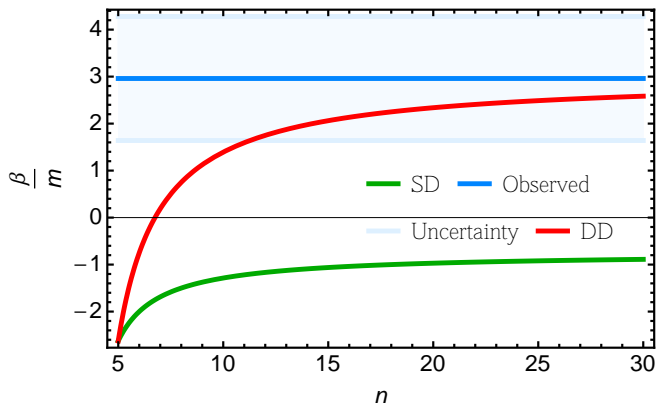


FIG. 2.— Value of the Surface Brightness Index ($\frac{\beta}{m}$, which is equal to $\frac{\dot{F}/F}{\dot{R}/R}$) observed from SNR G1.9 + 0.3 compared with the modeled relationship between $\frac{\beta}{m}$ and n for both the SD and DD cases (Equation 23). The plotted error margin is 2σ . Note that the prediction from the DD case enters the allowed region, while that from the SD case does not. We can use this to select the DD scenario and reject the SD scenario.

where,

$$\beta \equiv \frac{3(-54 + n(8 - 5s) + 25s)}{8(n - s)}. \quad (20)$$

When we inspect the cases for SD or DD scenarios we see a striking difference in how the flux scales with time.

$$F_\nu \propto \begin{cases} t^{-\frac{3(2+n)}{4(n-3)}} & \text{for SD (s=2),} \\ t^{3-\frac{4s}{4(n-3)}} & \text{for DD (s=0).} \end{cases} \quad (21)$$

We note that in the SD case flux decreases with time, but in the DD case flux can increase for explosions with steep ejecta profiles. This is a stark qualitative distinction.

4. SURFACE BRIGHTNESS INDEX FROM CHANDRA X-RAY OBSERVATIONS

Recent X-ray observations from Chandra (Reynolds et al. 2008; Borkowski et al. 2014) tell us that SNR G1.9+0.3 is expanding and has increasing flux. Borkowski et al. (2014) found that the flux increases at a rate of, $\dot{F}/F = 1.9 \pm 0.4\% \text{ yr}^{-1}$. Reynolds et al. (2008) measured that the supernova remnant is expanding at a rate $\dot{R}/R = 0.642 \pm 0.049\% \text{ yr}^{-1}$.

We know from Equation 10 that $\dot{R}/R = m/t$. We can see from Equation 19 that $\dot{F}/F = \beta/t$. The right hand sides of two relationships are derived from a theoretical standpoint. Their left hand sides can be determined experimentally as listed above. We can therefore eliminate the age of the remnant and solve for $\frac{\beta}{m}$. This will help us decide the correct circumstellar density profile and allowed values of the explosion index n , which can explain the evolution of the remnant. Therefore, from observations,

$$\frac{\beta}{m} \equiv \frac{\dot{F}/F}{\dot{R}/R} = 2.96 \pm 0.66. \quad (22)$$

We name this ratio, the Surface Brightness Index, since it relates flux and size evolution. It is a dimensionless number which measures how the brightness of the remnant evolves. Since it does not explicitly depend on the age, it can be determined from observations even when the date of explosion is unknown.

The Brightness Index can also be computed from theory. Using the Equations 11 and 20 for m and β we can write from theory,

$$\frac{\beta}{m} = \begin{cases} -\frac{3}{4} \times \frac{n^2-4}{(n-3)^2} & \text{for SD (s=2),} \\ \frac{3}{4} \times \frac{n(4n-27)}{(n-3)^2} & \text{for DD (s=0).} \end{cases} \quad (23)$$

For an expanding remnant, a negative Brightness Index represents a declining flux while a positive one denotes a rising flux. The two special cases of $\frac{\beta}{m} = 0$ and 2 represent a constant flux and a constant surface brightness respectively.

In Figure 2 we graph the observed values of $\frac{\beta}{m}$ (and its range of uncertainty) vs. n (using the relationships found in Equation 23). This allows us to see which model is acceptable and what value of n puts the preferred model in the observed band. Just from the equations we can see that $\frac{\beta}{m}$ will always be negative in the SD case, so it will never yield the observed result of simultaneously increasing flux and size. Thus a SD solution only predicts decreasing flux, which we know to be untrue from the observed data. After selecting the $s = 0$ case based on observations, we can find our allowed range of n . Using the chosen values of s and n we determine the age of the remnant in the next section.

5. AGE ESTIMATES

Having selected the DD explanation ($s = 0$), based on observations, we now have to pick a value of n . Many authors, including Chevalier (1982a), have used a power law profile with $n = 7$ following Colgate & McKee (1969). However, based on the recent X-ray observations (Borkowski et al. 2014) and comparison with our models in Figure 2 we notice that we needed a steeper ejecta profile governed by a larger value for n . From Figure 2 we notice that only models with values of $n \gtrsim 11.5$ would explain the data. We chose 12 as our fiducial value of n in the rest of this work.

5.1. DD Case

Now we determine the age of the remnant using our value of $n = 12$ and $s = 0$, for the DD case. To this end, we first find,

$$m = \frac{n-3}{n} = \frac{3}{4}. \quad (24)$$

We also know that,

$$\frac{\dot{R}}{R} = \frac{m}{t} = \frac{3}{4t} = 0.642 \pm 0.049\% \text{ yr}^{-1} \quad (25)$$

Solving for t we have,

$$t = 116.8 \pm 8.9 \text{ yr}, \quad (26)$$

and taking into account that this data was obtained in 2008, we can determine when the supernova exploded. So from this estimate the supernova occurred in 1892 ± 9 years.

We can also estimate the age using our equation for β and the change in flux over time. We know,

$$\frac{\dot{F}}{F} = \frac{\beta}{t} = \frac{7}{4t} = 1.9 \pm 0.4\% \text{ yr}^{-1}. \quad (27)$$

Solving for t in this case we have,

$$t = 92.1 \pm 19.37 \text{ yr}, \quad (28)$$

So from this estimate the supernova occurred in 1916 ± 19 years.

The weighted mean of these two ages is 109 ± 9 years, which gives an explosion date of around 1899 ± 9 . This is within the upper limit of 150 years proposed by Green et al. (2008).

5.2. SD Case

Even though the SD case was shown to be inapplicable to SNR G1.9.0.3, for a consistency check we will now determine the age in the SD scenario using $s = 2$. So to start once again we find m for this case.

$$m = \frac{n-3}{n-2} = \frac{9}{10} \quad (29)$$

In the same fashion as above we will first solve for the age using the value of

$$\frac{\dot{R}}{R} = \frac{m}{t} = \frac{9}{10t} = 0.642 \pm 0.049\% \text{ yr}^{-1}. \quad (30)$$

So,

$$t = 140.19 \pm 10.69 \text{ yr}. \quad (31)$$

Now using the relationship for how flux changes over time, we will solve for t again.

$$\frac{\dot{F}}{F} = \frac{\beta}{t} = \frac{-7}{6t} = 1.9 \pm 0.4\% \text{ yr}^{-1}, \quad (32)$$

Where $\beta = -\frac{7}{6}$. Thus,

$$t = -61.40 \pm 12.84 \text{ yr}. \quad (33)$$

This points to an explosion date in the future, which is absurd. This result is not physically plausible and merely shows again that the SD case cannot incorporate a rising flux.

6. FLUX AND SIZE EVOLUTION

Having picked the preferred scenario based on scaling relations, we can now explicitly compute the flux and size evolution. When $n = 12$ the following equations describe the progression of the supernova over time for the DD scenario. We start by looking again at what the circumstellar density is,

$$\rho_{cs} = \rho_0. \quad (34)$$

Next we enumerate the density of the supernova ejecta. We assume a broken power law profile where the slow part has a constant density and the fast part has a power law profile with $n = 12$. The profile is determined by the constant density and the velocity at the point of change. These two values are completely determined by the initial energy and the initial mass of the supernova ejecta. Here E_0 is the initial energy, v is the change over velocity, and M_0 is the initial mass.

$$\rho_{sn} = \frac{13.0E_0^{9/2}}{M_0^{7/2}t^3v^{12}} \quad (35)$$

We can compare this with the initial setup and see that the scaling is the same for $s = 0$, and $n = 12$. Next we can find the masses of the shocked circumstellar matter (M_1), and the ejected mass (M_2). These were found by integrating the respective densities over the relevant volumes.

$$M_1 = \frac{4}{3}\pi\rho_0R^3 \quad (36)$$

$$M_2 = \frac{18.2E_0^{9/2}t^9}{M_0^{7/2}R^9} \quad (37)$$

We again can see that these agree with the predicted scalings in Section 3.2.

Next the two pressures are found by multiplying the flux of momentum trying to cross the contact discontinuity. P_1 is the pressure of the shocked circumstellar matter,

$$P_1 = \frac{0.640\rho_0}{M_0^2} \left(\frac{\rho_0}{E_0^{9/2}M_0^{17/2}} \right)^{-1/6} t^{-1/2}. \quad (38)$$

P_2 is the pressure of the ejected mass that collides with the shocked circumstellar matter. Therefore,

$$P_2 = \frac{0.427\rho_0}{M_0^2} \left(\frac{\rho_0}{E_0^{9/2}M_0^{17/2}} \right)^{-1/6} t^{-1/2}. \quad (39)$$

We can then use Equation 7 to solve for the radius, which comes out as ,

$$R(t) = \frac{1.07}{M_0} \left(\frac{\rho_0}{E_0^{9/2}M_0^{17/2}} \right)^{-1/12} t^{3/4}. \quad (40)$$

As stated above, thermal energy is less than the initial energy, but increasing during this phase of the supernova. The kinetic energy lost due to the interaction with the circumstellar medium is the thermal energy,

$$E_{th} = \frac{2.56E_0^{15/8}\rho_0^{7/12}t^{7/4}}{M_0^{35/24}}. \quad (41)$$

We consider a fraction, f , of the total volume, to be filled with amplified magnetic fields. So the energy in the magnetic field is,

$$E_B = \frac{0.202B^2E_0^{9/8}ft^{9/4}}{M_0^{7/8}\rho_0^{1/4}}. \quad (42)$$

Assuming that a fraction (ϵ_B) of the thermal energy goes into producing this magnetic field, we get

$$B = \frac{3.56E_0^{3/8} \left(\frac{\epsilon_B}{f} \right)^{1/2} \rho_0^{5/12}}{M_0^{7/24}t^{1/4}}. \quad (43)$$

Similarly, to find the energy in the accelerated electrons, the number density of electrons considered is $N_0E^{-p}dEdV$ extending from $\gamma_m m_e c^2$ to infinity. These electrons are assumed to fill a fraction f of the spherical remnant with radius R . So the energy in the accelerated electrons is,

$$E_e = \frac{5.08E_0^{9/8}f(\gamma_m m_e c^2)^{2-p}N_0t^{9/4}}{M_0^{7/8}(p-2)\rho_0^{1/4}}. \quad (44)$$

Assuming this is a fraction (ϵ_e) of the total thermal energy we have,

$$N_0 = \frac{0.503E_0^{3/4}\epsilon_e(\gamma_m m_e c^2)^{p-2}(p-2)\rho_0^{5/6}}{fM_0^{7/12}t^{1/2}}. \quad (45)$$

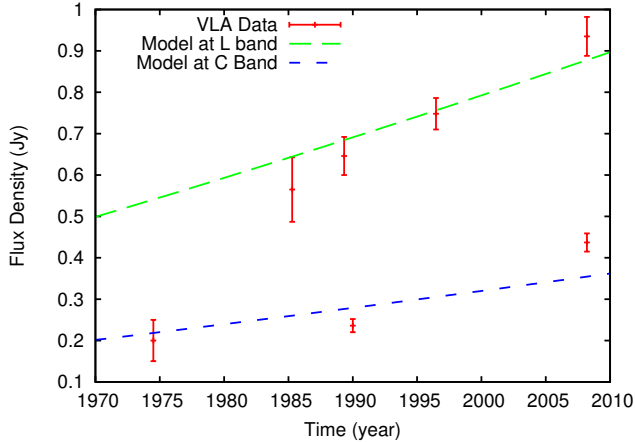


FIG. 3.— Flux densities from VLA radio observations of SNR G1.9+0.3 at L and C Bands compared with the best fit from the DD scenario (Equation 47). The data and the favored DD model, both show a rise. In contrast the disfavored SD model (Equation 49) would have predicted a decaying lightcurve.

Using Equation 17 and assuming $\epsilon_e = \epsilon_B = 0.01$ we have,

$$F_\nu = \frac{(8.260 \times 10^{-6}) c_5 E_0^{81/32} \left(\frac{c_1}{\nu}\right)^{3/4} (\rho_0 t)^{21/16}}{D^2 M_0^{63/32}}. \quad (46)$$

The flux depends directly on the initial energy and inversely on the distance to the supernova. It also increases with time and the initial density of the explosion, in a limited fashion.

7. PREDICTIONS FOR OBSERVED FLUX AND SIZE

Here we recast the equations from the previous section in units which can be used to conveniently predict fluxes and angular diameters, as determined by radio observations.

7.1. DD Case

First, the equation for the evolution of flux gives us,

$$F_\nu = 46.6 \left(\frac{t}{100\text{yr}}\right)^{1.31} \left(\frac{n_0}{\text{atom/cc}}\right)^{1.31} \left(\frac{E_0}{10^{51}\text{ergs}}\right)^{2.53} \times \left(\frac{\nu}{\text{GHz}}\right)^{-0.75} \left(\frac{D}{10\text{kpc}}\right)^{-2} \left(\frac{M_0}{1.4M_\odot}\right)^{-1.97} \text{ mJy}. \quad (47)$$

This equation shows that the flux depends most strongly on the initial energy of the explosion and rises with time.

Next the angular diameter, $\theta \equiv \frac{2R}{D}$, is given as

$$\theta = 42.7'' \left(\frac{t}{100\text{yr}}\right)^{0.75} \left(\frac{E_0}{10^{51}\text{ergs}}\right)^{0.38} \left(\frac{M_0}{1.4M_\odot}\right)^{-0.29} \times \left(\frac{n_0}{\text{atom/cc}}\right)^{-0.08} \left(\frac{D}{10\text{kpc}}\right)^{-1}. \quad (48)$$

So the angular diameter is most strongly affected by the distance from the observer to the SNR and the time since the explosion.

7.2. SD Case

Here we provide the corresponding versions of these equations, in convenient units, for the SD case. These are not used for SNR G1.9+0.3 but are provided for reference. First, the flux can be expressed as

$$F_\nu = 33.1 \left(\frac{t}{100\text{yr}}\right)^{-1.05} \left(\frac{\dot{M}}{10^{-7}M_\odot/\text{yr}}\right)^{1.58} \times \left(\frac{E_0}{10^{51}\text{ergs}}\right)^{1.35} \left(\frac{\nu}{\text{GHz}}\right)^{-0.75} \left(\frac{D}{10\text{kpc}}\right)^{-2} \times \left(\frac{M_0}{1.4M_\odot}\right)^{-1.05} \left(\frac{v_w}{100\text{km/s}}\right)^{-1.58} \text{ mJy}. \quad (49)$$

We can see from this equation that flux in this case strongly depends on the distance to the object, D . The rate of mass loss, \dot{M} and the velocity of the wind, v_w also affect the flux.

Next the angular diameter can be written as

$$\theta = 63.9'' \left(\frac{t}{100\text{yr}}\right)^{0.9} \left(\frac{E_0}{10^{51}\text{ergs}}\right)^{0.45} \left(\frac{M_0}{1.4M_\odot}\right)^{-0.35} \times \left(\frac{\dot{M}}{10^{-7}M_\odot/\text{yr}}\right)^{-0.1} \left(\frac{v_w}{100\text{km/s}}\right)^{0.1} \left(\frac{D}{10\text{kpc}}\right)^{-1}. \quad (50)$$

The angular diameter depends on the distance from the explosion, and the time since the explosion. There is also a large direct dependence on the initial energy.

We provide results for both the DD and SD scenarios so that they can be compared with future observations of other remnants to see which one more accurately models the observed evolution.

8. COMPARISON WITH VLA RADIO OBSERVATIONS

We can use the recent radio observations to estimate the size and flux of the supernova remnant. Equations 47 and 48 let us find how they depend on external density and initial energy. From Figure 2 in Green et al. (2008) that depicts the azimuthally averaged radial profile of the radio emission in 2008, we inferred a mean emission weighted radius of $\frac{\theta}{2} = 34.5''$ at an age of $t = 109$ yr. This observed size can be substituted into Equation 48 recast as,

$$\theta = 53.6'' E_{51}^{3/8} n_0^{-1/12}, \quad (51)$$

for the distance to the particular remnant and its age. In the above equation the only two unknowns are n_0 (in units of atoms/cc) and E_{51} (in units of 10^{51} ergs) as θ is known from observations.

From the Section 7 we can use Equation 47, with a value of flux (F_0) for observations at ~ 1 GHz. This can then be compared to the observed value from Green et al. (2008). We also use a distance $D = 8.5\text{kpc}$. We chose this as the distance to the supernova because we assume it is near the Galactic center. Time of the observations is measured from our fiducial explosion year of 1899. Mass of the explosion is assumed to be close to a Chandrasekhar mass. First we fit (See Figure 3) the

radio observation with,

$$F_\nu(t, \nu) = F_0 \left(\frac{(t - 1899)}{100\text{yr}} \right)^{21/16} \left(\frac{\nu}{1\text{GHz}} \right)^{-3/4} \text{Jy}, \quad (52)$$

to find F_0 , the flux density at age 100 years observed at 1 GHz. We did find that $F_0 = 1.03 \pm 0.05\text{Jy}$. Next we can plug this information into,

$$F_0 = 64.5 E_{51}^{81/32} n_0^{21/16} \text{mJy}. \quad (53)$$

Substituting the observed size and flux into the Equations 47 and 48, we can therefore solve for the density, (n_0), and the initial energy, (E_{51}). We found that the values, $n_0 = 1.8 \text{ atom/cc}$ and $E_0 = 2.2 \times 10^{51} \text{ ergs}$, when used in Equations 47 and 48, reproduce the observed flux and size evolution in the radio. We also note that these are reasonable values to expect for the density and initial energy. Note that these values should be seen as consistency checks rather than determinations of the density and energy, because of systematic uncertainties introduced by unknowns like ϵ_e and ϵ_B .

9. EFFECTS OF ELECTRON COOLING

The effects of electron cooling on broadband spectrum may become apparent when observing the spectrum in both the radio and the x-ray. Magnetic fields that permeate the SNR cause the electrons to lose energy, and cool down. This produces emission that can be described by a power law,

$$F_\nu \propto \nu^\alpha. \quad (54)$$

However, the radio and x-ray emission may not be explained by the same power law.

9.1. Spectral model

Above some critical Lorentz factor (γ_c) the electrons have lost enough energy that slope of the power law changes. According to Piran (1999) the slope before the critical Lorentz factor, possibly at the radio frequencies, is

$$\alpha = \frac{1-p}{2}, \quad (55)$$

where we chose p to be 2.5. Once the electrons' Lorentz factor is above γ_c the slope changes to (Piran 1999),

$$\alpha = \frac{-p}{2}. \quad (56)$$

The Lorentz factor, of radiating electrons, is related to a corresponding frequency (ν_c), of emitted photons. Following Rybicki & Lightman (1979), these can be related as,

$$\nu(\gamma) = \gamma^2 \frac{q_e B}{2\pi m_e c}, \quad (57)$$

where c is the speed of light, B is the magnetic field, and m_e mass of an electron. The critical Lorentz factor, above which synchrotron losses dominate, is given by (Sari et al. 1998),

$$\gamma_c = \frac{6\pi m_e c}{\sigma_T B^2 t}, \quad (58)$$

where σ_t is the Thomson cross-section, and t is the age of the remnant. This critical Lorentz factor comes out to be, $\gamma_c \sim 2 \times 10^5$ after evaluating the expression for SNR G1.9+0.3. Chakraborti & Ray (2011) expressed the relationship, between the critical frequency and Lorentz factor, as

$$\nu_c = \frac{18\pi m_e c q_e}{\sigma_T^2 B^3 t^2}, \quad (59)$$

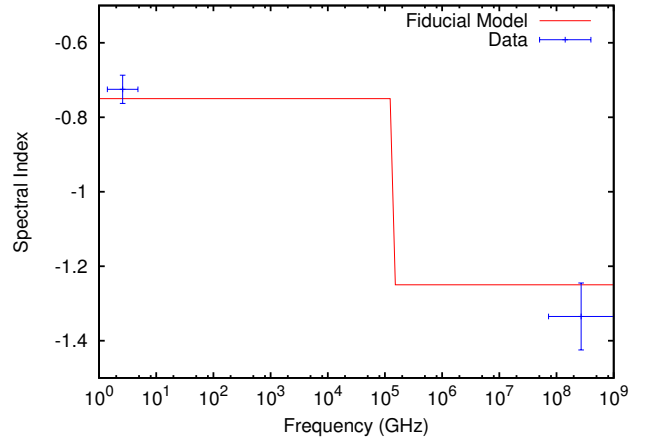


FIG. 4.— This graph, of the spectral index predicted by the fiducial model and that observed in the data, shows that the model can explain the two different spectral indices at radio and X-ray frequencies. Note that this is not a fit, but merely a graphical comparison of the predicted spectral indices with observed ones.

where q_e is the charge of an electron. Following this equation we found that $\nu_c = 1.3 \times 10^{14} \text{ Hz}$, so we expect that the value of α should change at infrared frequencies. We checked our estimates by increasing and decreasing the assumed density by a factor of 10 to see if it would affect the break where the spectrum changes slope. However, even after varying the density the break was still in the infrared. Therefore we expect to see change in slope somewhere between the radio and x-ray bands, probably in the infrared.

9.2. Observed Spectral Indices

The L and C band data from Figure 3 was used to determine the spectral index at radio frequencies. L band corresponds to frequencies near 4.8 GHz, while C band corresponds to 1.4 GHz in frequency. We found that the spectral index was $\alpha_{\text{radio}} = -0.725 \pm 0.091$

SNR G1.9+0.3 was observed with the Chandra X-Ray Observatory by a team (PI: Kazimierz Borkowski) in Observation 12691 on May 9, 2011. The ACIS-S chip was used for 184.0 ks. To use the data from the x-ray observations we first had to extract the spectra out of the image. Then we imported this spectra into XSPEC to further analyze it. We used the tbabs absorption model and a simple power law emission model to fit the data. We argue against using the srct model extending from radio to X-rays, because we expect a synchrotron cooling break below the x-ray band. We therefore fit the radio and X-ray data separately. The X-ray model was decided to be a good fit, by simulating 10,000 spectra where only 57% of realizations were found better than the observed spectra. We convert the photon index, as mostly used in X-ray analysis software, into the spectral index to compare with radio observations. We found that $\alpha_{\text{Xray}} = -1.335 \pm 0.045$.

Finally, in Figure 4 we plot the observed values of the spectral index and compare it with the predictions from our fiducial model. Note, that this is not a fit, but merely a comparison to show that our model naturally predicts the observed steepening in the spectral index from the radio to the x-rays.

10. DISCUSSIONS

We have shown that circumstellar interaction in young supernova remnants is an useful tool in trying to discern progenitors of thermonuclear supernovae. We have developed a new diagnostic, the Surface Brightness Index, relating flux and size evolution of remnants. In particular, we favor a DD scenario for SNR G1.9+0.3. Based on application of our models to SNR G1.9+0.3 we present here a prescription to evaluate other young supernova remnants that are observed in x-ray and/or radio. These recommendations would be helpful in deducing the nature and surroundings of a Type Ia supernova.

- Observe the flux density and size of the remnant to determine how they change in time.
- Re-construct Figure 2 and plot the observed ratio of the fractional changes in flux and radius.
- Compare this observed ratio with theoretical predictions for the Surface Brightness Index.
- Rule out either SD or DD scenarios.
- Use appropriate equations from Section 7, to determine explosion energy and circumstellar density.

Type Ia supernovae are responsible for much of the heavy elements in the universe and of fundamental importance as distance indicators in cosmology. In such a situation, identification of their progenitors is a matter of utmost concern. Opinion is divided mostly between SD and DD scenarios. In this work we have shown that circumstellar interaction in young supernova remnants can be a useful discriminator between these possibilities. We have used this technique to demonstrate that the

youngest Galactic supernova remnant SNR G1.9+0.3 is likely the product of a DD progenitor system. Our model shows that an SD scenario cannot produce a rising flux, whereas the DD case does. Our result shows that Type Ia supernovae can all have DD progenitors or a combination of SD and DD populations. The scenario in which all progenitors are SD is ruled out.

We suggest that further progress can be made by deep radio detections or tight upper limits, thanks to the increased sensitivity of the upgraded VLA, of historical Type Ia supernova in the local group. Radio observations of nearby Type Ia supernovae within a year of explosion (Chomiuk et al. 2015) put tight constraints on SD progenitor scenarios. Late observations will be particularly useful for constraining DD progenitor scenarios since they predict rising flux densities. Observations of SN 1885A in M31, SN 1895B in NGC5253 and SN 1937C in IC4182 with $\sim \mu\text{Jy}$ level sensitivity will be especially useful. Future observations of SN 2011fe are also important, even with the current upper limits (which puts pressure on SD scenarios) as the DD scenario predicts a rising lightcurve which may be detectable in the future. In absence of pre-explosion progenitor detections, for Type Ia supernovae, circumstellar interactions may provide the most important insights into their hitherto elusive progenitors.

ACKNOWLEDGEMENTS

We thank Alak Ray, Naveen Yadav, Roger Chevalier and Laura Chomiuk for discussions. This work made use of radio observations from the NRAO VLA. The National Radio Astronomy Observatory is a facility of the National Science Foundation operated under cooperative agreement by Associated Universities, Inc. The scientific results reported in this article are based in part on data obtained from the Chandra Data Archive.

REFERENCES

- Badenes, C., Hughes, J. P., Bravo, E., & Langer, N. 2007, *ApJ*, 662, 472, astro-ph/0703321
- Borkowski, K. J., Reynolds, S. P., Green, D. A., Hwang, U., Petre, R., Krishnamurthy, K., & Willett, R. 2014, *ApJ*, 790, L18, 1406.2287
- Borkowski, K. J., Reynolds, S. P., Hwang, U., Green, D. A., Petre, R., Krishnamurthy, K., & Willett, R. 2013, *ApJ*, 771, L9, 1305.7399
- Chakraborti, S., & Ray, A. 2011, *ApJ*, 729, 57, 1011.2784
- Chakraborti, S. et al. 2015, *ArXiv e-prints*, 1510.06025
- . 2013, *ApJ*, 774, 30, 1302.7067
- Chakraborti, S., Yadav, N., Ray, A., Smith, R., Chandra, P., & Pooley, D. 2012, *ApJ*, 761, 100, 1206.4033
- Chandrasekhar, S. 1931, *ApJ*, 74, 81
- Chevalier, R. A. 1982a, *ApJ*, 259, L85
- . 1982b, *ApJ*, 258, 790
- . 1982c, *ApJ*, 259, 302
- . 1984, *ApJ*, 285, L63
- Chevalier, R. A., Fransson, C., & Nymark, T. K. 2006, *ApJ*, 641, 1029, astro-ph/0509468
- Chomiuk, L. et al. 2015, *ArXiv e-prints*, 1510.07662
- . 2012, *ApJ*, 750, 164, 1201.0994
- Colgate, S. A., & McKee, C. 1969, *ApJ*, 157, 623
- Cowsik, R., & Sarkar, S. 1984, *MNRAS*, 207, 745
- Dwarkadas, V. V., & Chevalier, R. A. 1998, *ApJ*, 497, 807
- Filippenko, A. V. 1997, *ARA&A*, 35, 309
- Green, D. A., & Gull, S. F. 1984, *Nature*, 312, 527
- Green, D. A., Reynolds, S. P., Borkowski, K. J., Hwang, U., Harrus, I., & Petre, R. 2008, *MNRAS*, 387, L54, 0804.2317
- Hillebrandt, W., & Niemeyer, J. C. 2000, *ARA&A*, 38, 191, astro-ph/0006305
- Horesh, A. et al. 2012, *ApJ*, 746, 21, 1109.2912
- Iben, Jr., I., & Tutukov, A. V. 1984, *ApJS*, 54, 335
- Margutti, R. et al. 2012, *ApJ*, 751, 134, 1202.0741
- Minkowski, R. 1941, *PASP*, 53, 224
- Nomoto, K. 1982, *ApJ*, 253, 798
- Nomoto, K., Thielemann, F.-K., & Yokoi, K. 1984, *ApJ*, 286, 644
- Pacholczyk, A. G. 1970, *Radio astrophysics. Nonthermal processes in galactic and extragalactic sources*
- Perlmutter, S. et al. 1999, *ApJ*, 517, 565, astro-ph/9812133
- Phillips, M. M. 1993, *ApJ*, 413, L105
- Piran, T. 1999, *Phys. Rep.*, 314, 575, astro-ph/9810256
- Reynolds, S. P., Borkowski, K. J., Green, D. A., Hwang, U., Harrus, I., & Petre, R. 2008, *ApJ*, 680, L41, 0803.1487
- . 2009, *ApJ*, 695, L149, 0903.1870
- Riess, A. G. et al. 1998, *AJ*, 116, 1009, astro-ph/9805201
- Riess, A. G., Press, W. H., & Kirshner, R. P. 1996, *ApJ*, 473, 88, astro-ph/9604143
- Rybicki, G. B., & Lightman, A. P. 1979, *Radiative processes in astrophysics*
- Sari, R., Piran, T., & Narayan, R. 1998, *ApJ*, 497, L17, astro-ph/9712005
- Schmidt, B. P. et al. 1998, *ApJ*, 507, 46, astro-ph/9805200
- Smartt, S. J., Eldridge, J. J., Crockett, R. M., & Maund, J. R. 2009, *MNRAS*, 395, 1409, 0809.0403
- Webbink, R. F. 1984, *ApJ*, 277, 355
- Wheeler, J. C., & Harkness, R. P. 1990, *Reports on Progress in Physics*, 53, 1467
- Whelan, J., & Iben, Jr., I. 1973, *ApJ*, 186, 1007